Title

Influence of assimilating rainfall derived from WSR-88D radar on the rainstorm forecasts over the southwestern United States

Journal

Journal of Geophysical Research, 111(D13)

ISSN

0148-0227

Authors

Xu, Jianjun
Xiao, Qingnong
Gao, X
et al.

Publication Date

2006

DOI

10.1029/2005jd006650

Influence of assimilating rainfall derived from WSR-88D radar on the rainstorm forecasts over the southwestern United States

Jianjun Xu,[1,2] Qingnong Xiao,[3] X. Gao,[4] and S. Sorooshian[4]

Received 6 September 2005; revised 6 February 2006; accepted 24 March 2006; published 8 July 2006.

[1] In this study, the impact of rainfall assimilation on the forecasts of convective rainfall over the mountainous areas in the southwestern United States is investigated. The rainfall is derived from the U.S. Weather Surveillance Radar–1988 Doppler (WSR-88D) radar network, and the fifth-generation Mesoscale Model (MM5) Four-Dimensional Variational (4DVAR) system is employed in the study. We evaluate the rainfall assimilation skill through two rainstorm events (5–6 August and 11–12 September 2002) that occurred over the southwestern United States in 2002. A series of experiments for the two cases is conducted. The results show that the minimization process in the 4DVAR is sensitive to the length of assimilation window and error variance in the observation data. Assimilation of rainfall can produce a better short-range precipitation forecast. However, the time range of improved forecasts is limited to about 15 hours with the model resolution of 20 km. It is indicated that rainfall assimilation produces more realistic moisture divergence and temperature fields in the initial conditions for the two cases. Therefore the forecast of rainstorms is closer to observations in both quantity and pattern.

Citation: Xu, J., Q. Xiao, X. Gao, and S. Sorooshian (2006), Influence of assimilating rainfall derived from WSR-88D radar on the rainstorm forecasts over the southwestern United States, *J. Geophys. Res.*, *111*, D13105, doi:10.1029/2005JD006650.

1. Introduction

[2] The southwestern United States receives over 50% of its annual precipitation from June to September from the North American monsoon system [*Douglas et al.*, 1993; *Okabe*, 1994; *Stensrud et al.*, 1995; *Adams and Comrie*, 1997; *Anderson and Roads*, 2002; *Zeng and Lu*, 2004; *Xu et al.*, 2004a]. The high spatial variability of monsoon rainfall viewed from high-resolution satellite remote sensing [*Negri and Adler*, 1993; *Negri et al.*, 1994] indicates that the great complexity of the rainfall distribution is related to the mountainous topography of the region. With the arrival of the maritime tropical air mass associated with the North American monsoon system (NAMS), extreme storms can occur through the deep convection over the mountain slopes and can result in hydrological disasters such as flash flooding [*Farfan et al.*, 1998]. Improving the forecasts of monsoon rainfall in the southwestern United States therefore has received a great deal of attention in the hydrometeorological community.

[3] It has also been observed for a lengthy period in the operational centers that the loss of skill in weather forecasts does not occur at the same leading time every day [*Toth and Kalnay*, 1993]. One reason for the failure of weather forecasts can be attributed to the imperfection of numerical modeling in representing the actual atmosphere. However, as *Lorenz* [1963] pointed out, the most fundamental cause of forecast failure is because the atmosphere is a chaotic system. A chaotic system is defined as one in which evolution is sensitive to initial conditions (ICs). It means that an arbitrarily small error in the analysis of the initial state of the atmosphere can have an overwhelming effect in a finite amount of time. Therefore it is not surprising that considerable effort has focused on improving the estimates of the model initial states through advanced techniques. One such technique is the Four-Dimensional Variational (4DVAR) data assimilation method.

[4] The major advantage of 4DVAR is the use of full model dynamics and physics to assimilate multiple-time-level observation data (instead of assimilating observation data only at the initial time). The important components of the 4DVAR system are the tangent linear model (TLM), derived from the original forecast model, and its corresponding adjoint model (ADM). However, the usefulness of the TLM and ADM is only valid in a ''short'' time period, that is, the linearity valid period. In the 4DVAR procedure, a cost function is set to measure the difference (distance) between the model-simulated and observed fields of atmospheric variables. The minimization of the cost function is achieved through iterative runs of the forecast model with the model ICs according to the gradients calculated from the ADM. Obviously, the resulting ICs through the minimization procedure are not only fitting to the observations, but also consistent with the dynamics and physics of the forecast system [*Lewis and Derber*, 1985; *Le*

[1]Department of Hydrology and Water Resources, University of Arizona, Tucson, Arizona, USA.
[2]Joint Center for Satellite Data Assimilation, Camp Springs, Maryland, USA.
[3]National Center for Atmospheric Research, Boulder, Colorado, USA.
[4]Department of Civil and Environmental Engineering, University of California, Irvine, California, USA.

0148-0227/06/2005JD006650

Dimet and Talagrand, 1986; *Talagrand and Courtier*, 1987; *Zou and Kuo*, 1996; *Li et al.*, 2000].

[5] Many studies indicate that the divergence and moisture in the initial conditions of numerical modeling are the key ingredients affecting the intensification of precipitation over the extratropical regions [*Uccellini*, 1991; *Davidson and Puri*, 1992; *Petty and Miller*, 1995]. Rainfall assimilation via 4DVAR has been used in several studies to improve the moisture distributions in model ICs and has obtained encouraging forecasting results [*Zupanski and Mesinger*, 1995; *Zou and Kuo*, 1996; *Xiao et al.*, 2000; *Xu et al.*, 2004b]. Using 4DVAR to generate model ICs, the precipitation intensity and patterns can be improved over the midlatitude plain regions [*Zupanski and Mesinger*, 1995; *Zou and Kuo*, 1996; *Alexander et al.*, 1999] as well as the tropical regions [*Tsuyuki*, 1997]. However, it is a challenge to improve rainfall forecasts over the mountainous southwestern United States. First, in contrast to the precipitation over the plain areas, the cumulus convection plays a dominant role in determining the local atmospheric flow in the mountainous areas. Rising motion forced by mountains may lead to torrential rainfall. Mountains may also enhance rainfall by modulating the low-level convergence associated with flow deflection around the topography [*De Pondeca and Zou*, 2001; *Colle and Mass*, 1996] and by triggering the instability of convection [*Smith*, 1979]. This property makes it essential to include an appropriate cumulus convection parameterization and a reasonable horizontal resolution in the 4DVAR system in order to improve rainfall forecasts in mountainous regions. Because the physical processes depend strongly on the spatial resolution and are far more nonlinear than the dynamics, the tangent-linear approximation will make a big difference in different physical parameterizations and spatial resolutions. These nonlinear features will degrade the efficiency of commonly used minimization algorithms. This is one of the problems to be encountered when applying 4DVAR to mountainous regions. Associated with the nonlinearity and discontinuity in the 4DVAR system, the length of assimilation window is an issue which needs to be taken into account. Because of the lack of accurate estimation in the background error and observation errors, the length of assimilation has an impact on the iteration of the minimization process in 4DVAR experiments [*Zupanski and Mesinger*, 1995]. Another problem in the mountainous region is the poor quality and coverage of ground-based rainfall measurements. Most existing rain gauge networks are located in accessible low-elevation areas so that large gaps in information exist for the mountainous areas where considerable precipitation occurs. The NEXRAD (next general weather radar) radar coverage is also limited by mountain blockage of the low-radar beams, while the precipitation estimates derived from high-radar beams are less correlated with surface rainfall [*Maddox et al.*, 2002].

[6] In addition to research to improve the dynamics and physics of forecast models, the effectiveness of the data assimilation technique should be studied. Two basic questions arise here: Will the rainfall assimilation affect the rainfall forecasts in the mountainous southwestern United States using the 4DVAR approach? How does the assimilation time window and observation error in the 4DVAR procedure affect the rainfall forecasts?

[7] In this paper, two typical strong rainfall events that occurred in the southwestern United States on 5–6 August and 11–12 September 2002 are studied. A series of numerical experiments with alternative selections of assimilation time windows in Case 1 and the weighting of observations in Case 2 with the fifth-generation Mesoscale Model–Four-Dimensional Variational (MM5-4DVAR) system are conducted, and their influences on weather forecasts are analyzed.

[8] A brief overview of the MM5 data assimilation and forecasting system is given in the following section. The major characteristics of the WSR-88D (Weather Surveillance Radar–1988 Doppler) rainfall data are described in section 3. The results from the rainfall events on 5–6 August (Case 1, hereafter) and 11–12 September (Case 2, hereafter) are presented in sections 4 and 5, respectively. Further analysis and discussion of the results are presented in section 6. Finally, a summary and discussion are given in section 7.

2. MM5 4DVAR Assimilation and Forecasting System

2.1. MM5 Forecast Model

[9] The Pennsylvania State University/National Center for Atmospheric Research (PSU/NCAR) fifth-generation Mesoscale Model MM5 [*Dudhia*, 1993; *Grell et al.*, 1994] is used in this study. MM5 is a limited area, nonhydrostatic mesoscale atmospheric model with terrain-following vertical coordinates (σ).

[10] The initial and boundary conditions are analyzed from the NCEP operational Eta model analysis. The lateral boundary conditions are time-dependent; they are changed every six hours from the Eta analysis. The planetary boundary layer (PBL) employs the high-resolution Blackadar scheme. Land use at each grid point is defined among 24 categories (ranging from urban land to snow or ice), with climatological values of associated physical properties (albedo, moisture availability, emissivity, roughness length, and thermal inertia) assigned according to the category and time of the year [*Grell et al.*, 1994].

[11] There are a wide variety of physical parameterization schemes available in the MM5 modeling system. In the previous work [*Xu and Small*, 2002], we compared results from a different combination of two convection schemes (Grell and Kain-Fritsch) and three radiation schemes (Community Climate Model, version 2 (CCM2), Cloud, and Rapid Radiative Transfer Model (RRTM)). Differences in simulated rainfall produced by the various combinations of schemes are substantial. The Grell-RRTM simulation produces the most realistic patterns and magnitudes of rainfall, including intraseasonal variations and the differences between the wet and dry year. Simulations using the Kain-Fritsch scheme produce too much rainfall and fail to represent the typical, observed decrease in precipitation from June to July. The CCM2 radiation scheme produces a simulated climate that is too cloudy, yielding little rainfall in the North American monsoon system (NAMS) region, regardless of the convection scheme used. Consequently, the Grell cumulus convective parameterization and RRTM radiation schemes were considered most appropriate when

describing the precipitation over the southwestern United States.

2.2. MM5-4DVAR

[12] The MM5-4DVAR system [*Zou et al.*, 1998] is employed in this study. To perform rainfall assimilation, the *Grell* [1993] cumulus parameterization and the *Dudhia* [1989] explicit moisture scheme with simple ice are included in the forward model and backward adjoint during its minimization procedure.

[13] The 4DVAR processing is carried out through minimization of the following cost function:

$$J(x_0) = \frac{1}{2}(x_0 - x_b)^T W (x_0 - x_b) + \frac{1}{2}\sum_{r=0}^{n} (H_r(x_r) - y_r)^T \cdot W_r (H_r(x_r) - y_r) + Jc,$$

where the first term is the background partial cost function that measures the distance between the model initial state (x_0) and all available information prior to the assimilation period, summarized by the background field (x_b). The model initial condition (x_0) is the control variable in the 4DVAR. They include eight three-dimensional fields: the wind components u, v; temperature T; specific humidity q; pressure perturbation p'; vertical velocity w; cloud water q_c; and rainwater q_r. The background field (x_b) has the same components as x_0. In this study, the background field (x_b) is interpolated from the operational Eta model analyses field. $\mathbf{W}$ is the weighting from the background. Theoretically, the value of $\mathbf{W}$ equals $\mathbf{B^{-1}}$, where $\mathbf{B^{-1}}$ inverses background error covariance matrix $\mathbf{B}$. On the basis of the National Meteorological Center (NMC) method, $\mathbf{W}$ is calculated as the inverse of the squared maximum difference between two forecasts that are 6 hours apart.

[14] The second term in the cost function measures the discrepancy between the model-predicted and radar-retrieved precipitation. $r = 1, 2, \ldots, n$, n is the total number of time levels on which the observed rainfall data are available. Vector $\boldsymbol{x}_r$ is the model state at time t_r, H_r is the observation operator that calculates rainfall at the observation sites, in which the Cressman-type objective analysis scheme [*Benjamin and Seaman*, 1985] is used to interpolate the sum of *Dudhia* [1989] microphysics precipitation and *Grell* [1993] cumulus precipitation to the observation sites, and y_r is the observed precipitation. $\mathbf{W_r}$ in the cost function represents the weighting from the rainfall observation at $t = t_r$, which is the inverse of observation error variance and is treated here to be stationary and diagonal (i.e., no correlations between the observations and the weightings do not vary in time, $\mathbf{W_r}$ = constant).

[15] The Jc term is a dynamical constraint term included in the procedure to increase the balance in the analysis. We do not intend to study the dynamical constraint term in this paper and, for clarity, we will eliminate it in the following discussion.

[16] The minimization algorithm used in this study is the limited-memory quasi-Newton method developed by *Liu and Nocedal* [1989]. After obtaining the optimal initial conditions, forward runs are started from the optimal initial conditions using MM5 version 3.5. All forecast experiments are integrated for a 12-hour period.

3. Precipitation Estimated From WSR-88D Radar

[17] A prototype, real-time, hourly, multisensor National Precipitation Analysis (NPA) has been developed at NCEP (National Center for Environmental Prediction) in cooperation with the Office of Hydrology (OH). Hourly digital precipitation (HDP) radar estimates are created by the WSR-88D Radar Product Generator on a 131 × 131 4-km grid centered over each radar site. The first product with a completed prototype was the national mosaic of radar precipitation HDP estimates. This radar-only product consists of nearly 100 WSR-88D radars which report to NCEP in real time via the Advance Weather Interactive Processing System (AWIPS). Each individual radar estimate is merged together on the national Hydrologic Rainfall Analysis Project (HRAP) grid, and the bins which contain more than one radar estimate are averaged together using a simple inverse distance weighted average. As a part of the National Weather Service (NWS) conversion from Automotion of Field Operational and Services (AFOS) to AWIPS during September 1999 to August 2000, the radar precipitation products from the 137 radar sites over the continental United States (CONUS) were converted from the HDP to the Digital Precipitation Array (DPA) format. There are currently two types of radar-only estimates: biased and unbiased. The radar bias removal algorithm follows *Smith and Krajewski* [1991]. The unbiased radar estimates are available after a ~6-hour delay to allow gauge data necessary to compute the biases to arrive. For more information, please refer to *Fulton et al.* [1998].

4. Case 1

4.1. Event

[18] From radar rainfall data and the operational Eta model analysis, a strong rainstorm occurred over southern Arizona with maximum rainfall of 35 mm/h in the vicinity of Tucson during 0500–0600 UTC 6 August 2002. At 2100 UTC 5 August 2002, a strong trough at 500 hPa was located on the western coast of North America, and the subtropical high with a 588-isobar line covered the east-central portion of the United States (not shown). In Figure 1a, the NCEP Eta analysis indicates that southeastern Arizona was dominated by southeastern winds with convergence at 700 hPa. In contrast, eastern New Mexico was dominated by a divergence. As a result of this circulation, the Gulf of Mexico was the primary moisture source for this convective process. At 2100 UTC, the radar data showed that a weak rainstorm occurred in eastern Tucson (Figure 1d). Afterward, the deep convective system moved westward. By 0300 UTC 6 August, the strong convergence center shifted westward (Figure 1b). Correspondingly, a well-defined rainband shifted westward to the area around Tucson (Figure 1e). At 0900 UTC, the convective system moved northeastward (Figure 1c), and a weak rainfall center appeared over northeastern Tucson (Figure 1f).

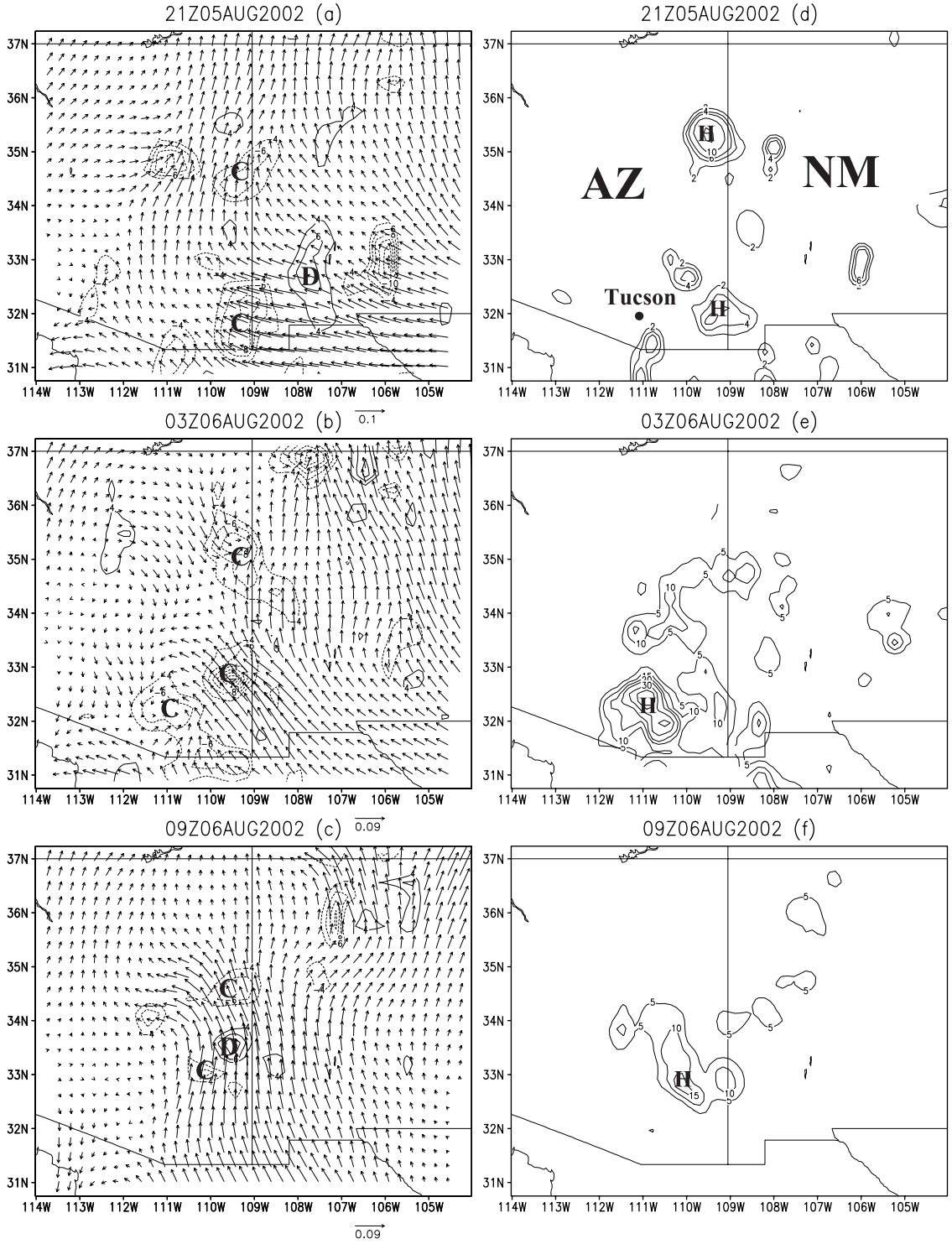

Figure 1. Divergence field (dashed lines, units 10^{-5}/s) and moisture transport vector ($\mathbf{u} \times \mathbf{q}$; $\mathbf{v} \times \mathbf{q}$) (units g/kg $\times$ m/s) at 700 hPa at (a) 2100 UTC 5 August, (b) 0300 UT 5 August, and (c) 0900 UTC 6 August 2002 (C, convergence; D, divergence). Rainfall (mm) at (d) 2100 UTC 5 August, (e) 0000 6 August, and (f) 0300 UTC 6 August 2002 (H, high center of rainfall).

[19] Obviously, the convective rainstorm intensified and moved steadily westward during the first 6 hours (Figures 1d and 1e). The convection center matched with the convergence center of moisture flow (Figures 1a and 1b), and the convective rainstorm was weakened during the second 6 hours. The atmospheric conditions indicate that an accurate divergence field was crucial to the mesoscale convective system.

4.2. Experimental Design

[20] Because the storms occurred largely during the period of 0000–0300 UTC 6 August 2002 over both Arizona and

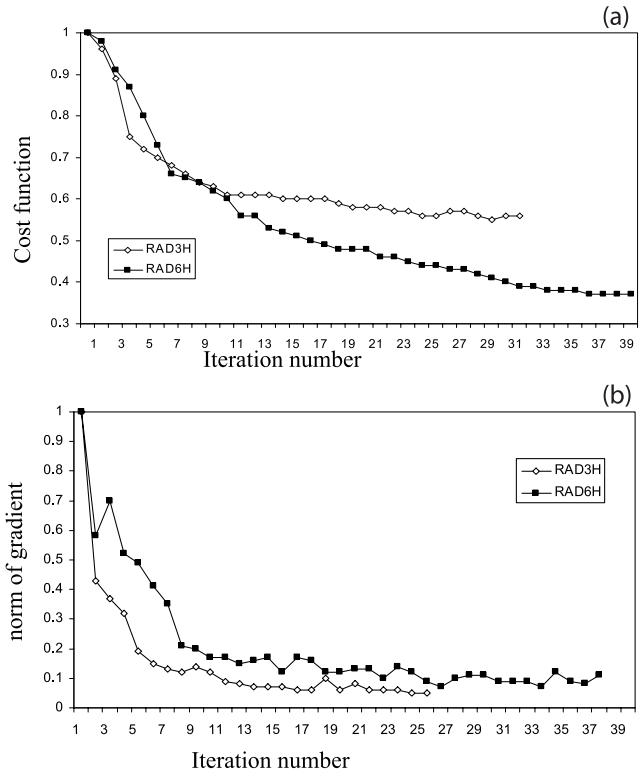

Figure 2. (a) Cost function and (b) norm of the gradient with respect to the number of iterations in the 4DVAR experiments.

New Mexico (Figure 1), we selected 2100 UTC 5 August as the initial time for simulation. An experiment with the MM5 forecast model represents a standard 12-hour model forecast run starting at 2100 UTC 5 August without data assimilation (NO4DVAR). This experiment is used as a benchmark to compare with other 4DVAR experiments. Two 4DVAR experiments were carried out with different assimilation windows (3 hour or 6 hour). All of the experiments were conducted at 20-km horizontal resolution. The two 4DVAR experiments are as follows: for RAD3H, use radar-derived rainfall data with a 3-hour assimilation window, and for RAD6H, use radar-derived rainfall data with a 6-hour assimilation window.

4.3. Performance of Rainfall Assimilation

4.3.1. Minimization Convergence

[21] The rate of gradient norm reduction is a measure for the convergence of the 4DVAR minimization. In Figure 2, the gradient norm is represented as a function of the number of iterations and, with approximately 10 iterations, the gradient norms in all experiments reduce by 80%. It demonstrates that the minimization in the MM5-4DVAR system converges well with the Doppler radar retrieved rainfall assimilation.

4.3.2. Rainfall Forecast

[22] In this case, the rainfall was concentrated in the Tucson area during the first 6 hours (from 2100 UTC 5 August to 0300 UTC 6 August). It then shifted northeastward during the second 6 hours (from 0300 to 0900 UTC 6 August). In order to show the effectiveness of rainfall assimilation, the rainfall forecasts from the 4DVAR experiments are compared with the NO4DVAR forecasts in these two successive 6-hour periods. In Figure 3, the forecasts of accumulated rainfall for the first 6 hours from experiments NO4DVAR and RAD3H are compared. The results show that the forecast of NO4DVAR does not determine the correct location of the storm: the rainfall center shifts northeastward to the area close to the Arizona–New Mexico border (compare Figure 3a with Figure 1e). In contrast, the forecast from the 4DVAR experiments improves the rainfall distribution over southeastern Arizona and reduces the substantial overestimation of rainfall amount in the NO4DVAR forecast (compare Figure 1e with Figure 3b). The rainfall forecasts in the second 6-hour period are illustrated in Figure 4. The NO4DVAR experiment produced three rainfall centers in southeast Arizona (Figure 4a) compared with only one rainfall center in the observations (Figure 1f). The rainfall forecasts from the 4DVAR experiments (Figure 4b) show better patterns and reduce rainfall

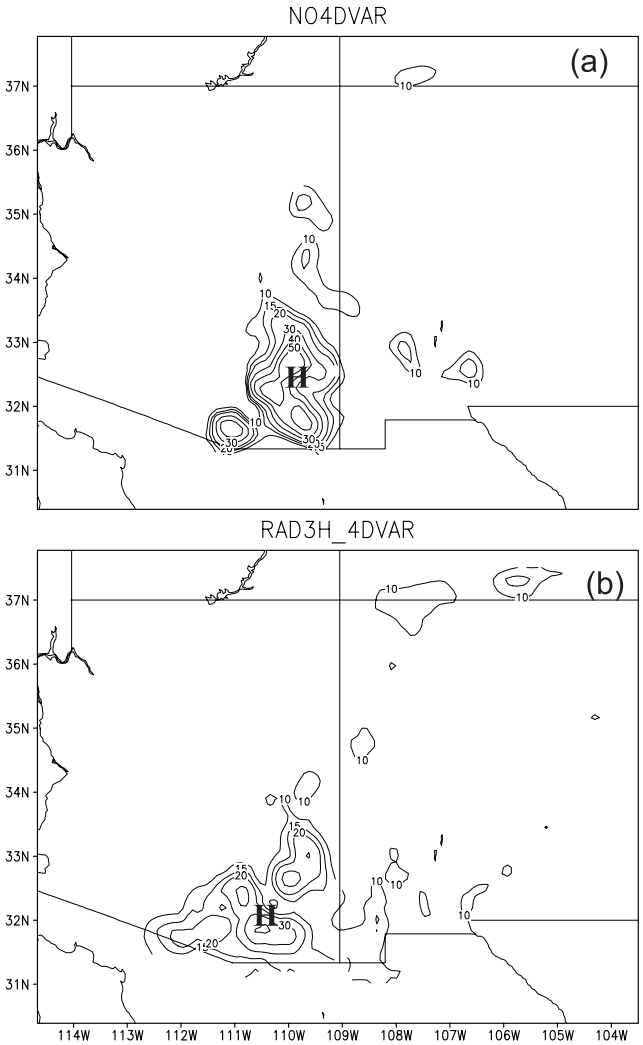

Figure 3. Six-hour accumulated precipitation of model simulation during the first 6-hour rainfall (mm) (2100 UTC 5 August to 0300 UTC 6 August 2002): (a) NO4DVAR and (b) RAD3H_4DVAR.

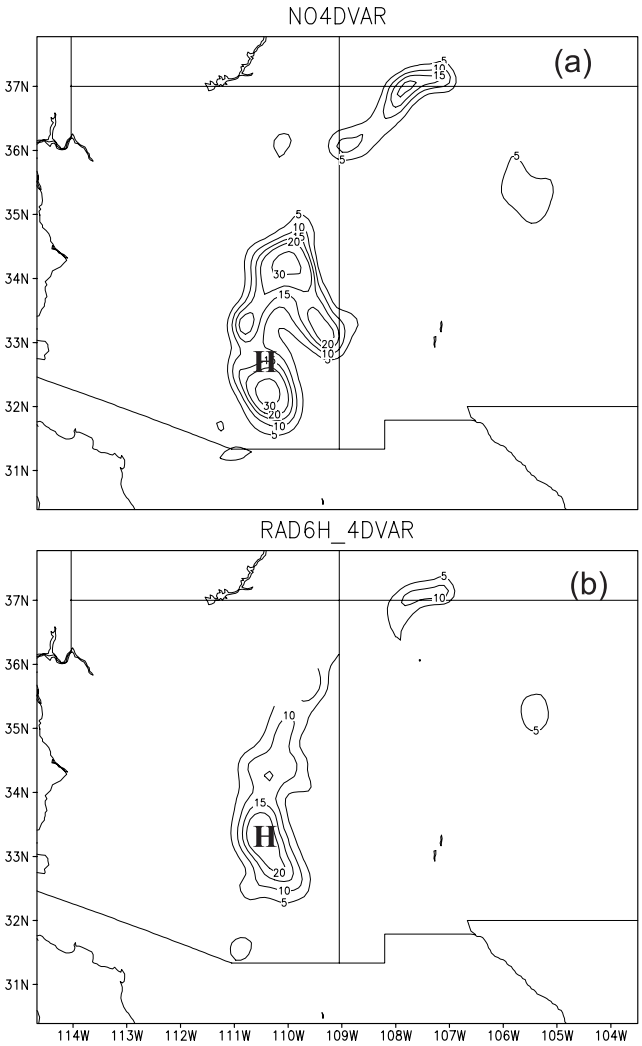

Figure 4. Six-hour accumulated precipitation of model simulation during the second 6- hour rainfall (mm) (0300∼0900 UTC 6 August 2002): (a) NO4DVAR and (b) RAD6H_4DVAR.

amounts than the NO4DVAR does, although they are still overestimated. In Figure 5, the curves for rainfall accumulations within the heavy rainfall area (109°–111.5°W, 31.5°–33°N) during the 12-hour forecast are plotted, which shows that all assimilation experiments produce more precipitation than the observation, but the forecasts made by the 4DVAR runs have smaller errors than the NO4DVAR prediction.

4.3.3. Sensitivity to Assimilation Time Window

[23] In order to explore the forecast performance with respect to the assimilation time window, the correlation and RMSE of forecasted rainfall against observed rainfall in the experiments with 3-hour assimilation window and 6-hour assimilation window are compared (Table 1). The statistics show that, for 6-hour rainfall forecasts, using a 3-hour assimilation window resulted in a higher correlation coefficient and a lower RMSE rather than using a 6-hour assimilation window unanimously. For 12-hour forecasts, however, opposite conclusions were displayed: using a

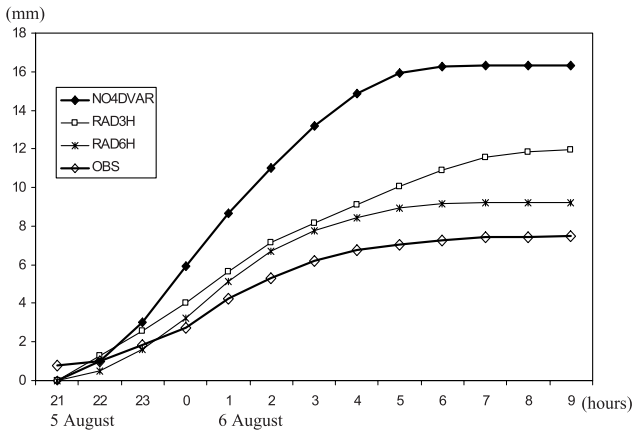

Figure 5. Time series of accumulated rainfall (mm) averaged over the rainstorm center (111.5°–109°W, 31.5°–33°N).

6-hour assimilation window provided better rainfall forecasts. Many previous studies have shown that the assimilation window should not be too long because of the chaotic nature of the atmosphere and the limited accuracy of the first-order linearization approximation [*Stensrud and Bao*, 1992; *Vukicevic and Bao*, 1998]. The optimal length of an assimilation window may depend on the model grid resolution, physical parameterization, and forecast duration. Our results suggest that the 3-hour assimilation window worked well for 6-hour forecasts using the MM5-4DVAR system in this case study, while for 12-hour or longer forecasts, a 6-hour assimilation window should be used.

5. Case 2

5.1. Event and Experimental Design

5.1.1. Event

[24] From radar rainfall data, a strong rainstorm occurred over the Mogollon Rim mountainous areas in the interface of northeastern Arizona and New Mexico on 10–11 September 2002, with a 6-hour total rainfall amount of 90 mm. Figure 6a shows that the location of the 6-hour rainfall centers (shaded with the amount of rainfall greater than 20 mm) lies roughly over the mountains with an elevation height of more than 1800 m. The time series of hourly precipitation (Figure 6b) averaged over the grid mesh

Table 1. RMSE and Correlation Coefficient Calculated Between Simulated and Observed Precipitation Over the Whole Studied Areas in the 6-Hour Forecast and 12-Hour Forecast[a]

	No 4DVAR	3 Hour Rad	6 Hour Rad
		First 6 Hours	
CORR	0.42	**0.48**	0.24
RMSE	8.67	**4.77**	6.64
		Second 6 Hours	
CORR	0.35	0.10	**0.51**
RMSE	4.97	3.79	**2.71**

[a]Rad is the radar precipitation data assimilation experiment and CORR is correlation coefficient.

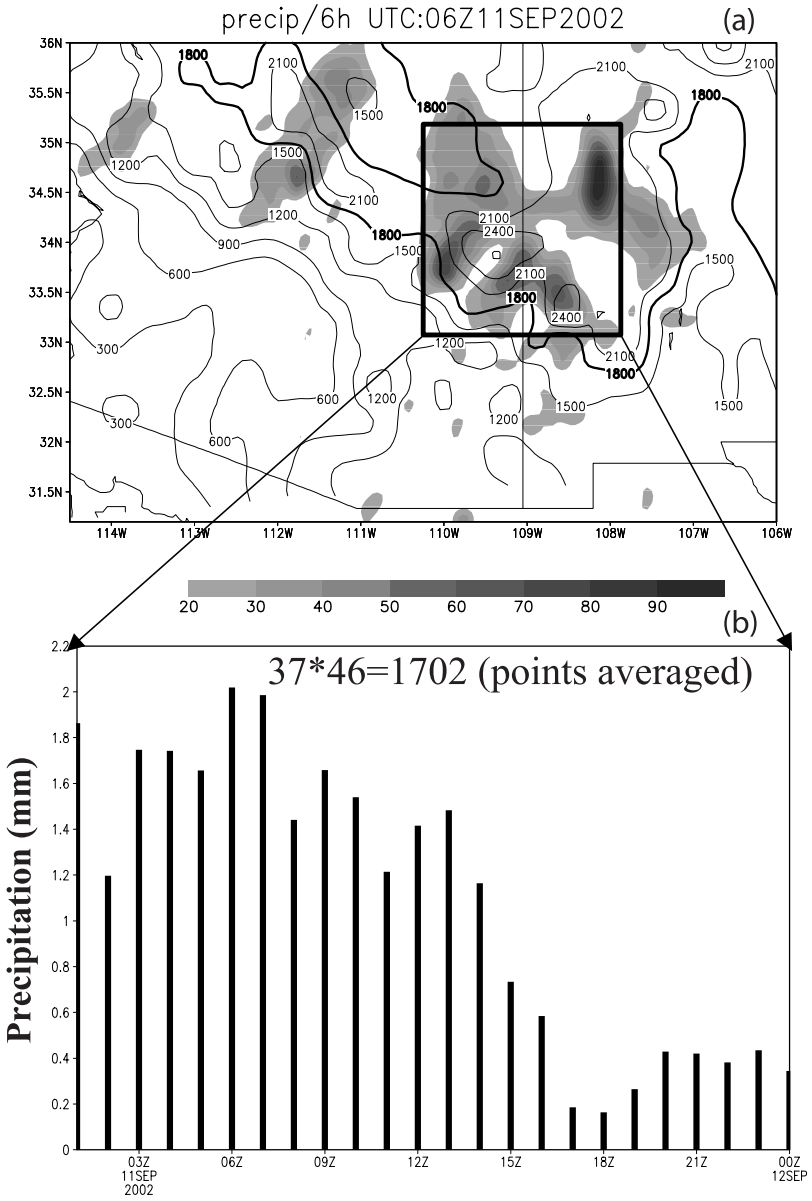

Figure 6. (a) Rainfall (mm) at 0600 UTC 11 September 2002 and (b) time series of hourly rainfall over the rainstorm central areas (heavy box in Figure 6a).

($37 \times 46 = 1702$ points) of the top mountain region (subset box in Figure 6a) indicates several peaks of hourly precipitation over 0 mm/h in the northern part of the Mogollon Rim.

[25] The NCEP Eta analysis is used as the first guess, and the objective analysis is based on the Cressman-type scheme. Figure 7 presents the analyzed upper level (300 hPa), lower level (700 hPa) divergence, and moisture transport vectors at 0000 UTC 11 September. During the initial stage of development, the upper level southerly flows with divergence across the mountainous area. The lower level moist air in the mountainous area originated from two directions: one from the Gulf of Mexico with southwest flow, and another from the eastern Pacific Ocean. Two branches of moist flows merge into the mountainous area and form a strong convergent flow. The vertical couplet structure (divergence at upper level and convergence at lower level) enhances convective instability that benefits the rainstorm occurrence in the following period.

5.1.2. Basic Idea and Experimental Design

[26] In 4DVAR data assimilation, a model is used as a strong constraint during minimization. The premise condition for the 4DVAR method is the perfect model assumption. In this study, we use fixed background error statistics (B) and conduct several experiments to examine the impact of various observational errors on the 4DVAR analysis and subsequent prediction.

[27] In fact, the weight of observation in the cost function is a tunable parameter that depends on the observational error variances [*Desroziers and Ivanov*, 2001]. The reported atmospheric observations used in data

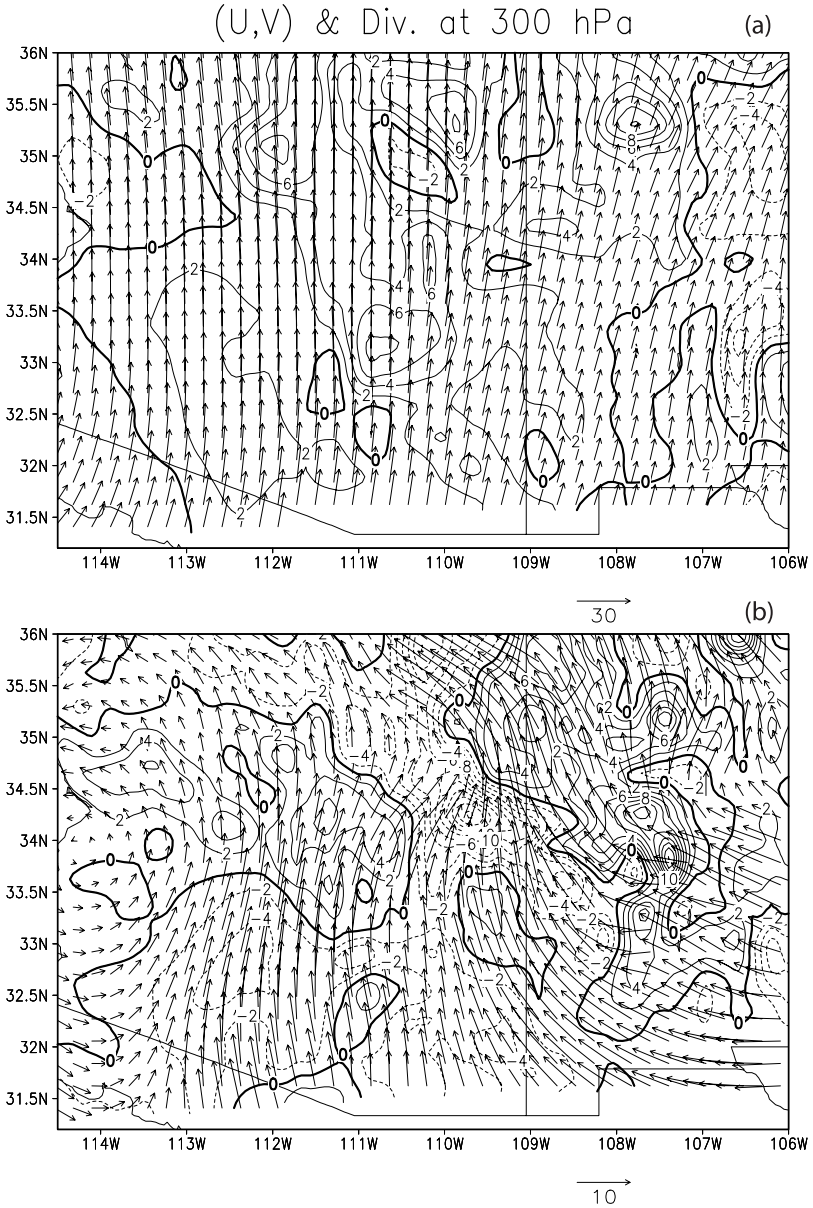

Figure 7. Divergence field (dashed lines, units 10^{-5}/s) and moisture transport vector ($\mathbf{u} \times \mathbf{q}$; $\mathbf{v} \times \mathbf{q}$) (units g/kg $\times$ m/s) at (a) 300 hPa and (b) 700 hPa.

assimilation are not perfect; they contain several kinds of errors, including instrumental errors and errors of human origin. The observations may contain errors which are so large that the observations have no useful information content and should be thrown out. Usually, the rough or gross errors which are of human origin and which take place during the computation or transmission of observation are difficult to evaluate. Experiments on multiple options for the weight of observation error can give statistical information on the observational error to be assigned.

[28] On the basis of the above idea, a series of tuning weights (W) of observational rainfall are assigned by the value of 0.25, 0.50, 0.75, 1.00, 1.25, 1.50, 1.75, 2.00, 2.25, 2.75, and 3.00×10^7 mm^{-2}. The MM5 4DVAR analyses and numerical predictions are carried out to assess the impact of the assigned weightings on the results of the analyses and predictions.

5.2. Minimization Performance

5.2.1. Cost Function

[29] The total cost function is contributed by terms of both background and observed rainfall. The weight of background error is a simple diagonal matrix, and the contribution of the background error does not change with the iteration of the minimization processes. In order to measure the relative contributions of background and observation (rainfall) terms to the total cost function, the ratio of observation to background in cost function value is used here. Figure 8a shows that the ratio at the initial time is in direct proportion to the weight of observation error. When the observation term is larger than the background term, the

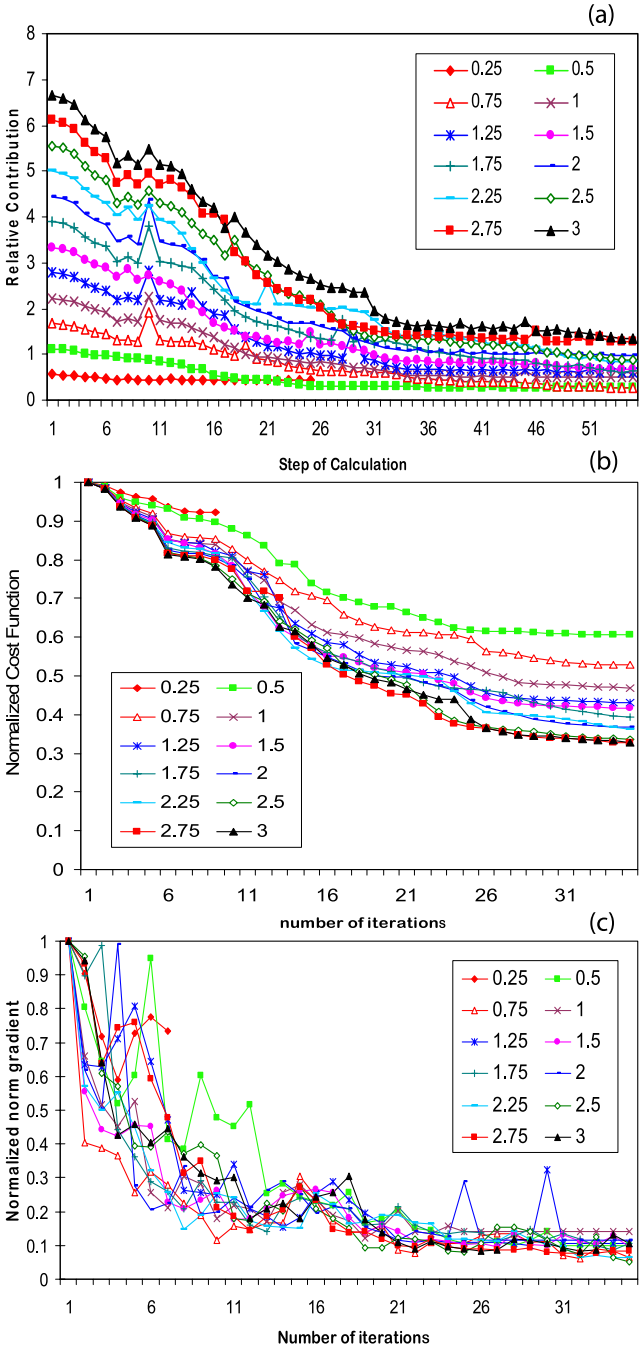

Figure 8. (a) Ratio of weights of background and observation error, (b) cost function, and (c) norm of the gradient with respect to the number of iterations in the 4DVAR experiments.

ratio is reduced more with the iteration of minimization processes. The larger the observational weight, the faster the ratio is reduced. On the other hand, by increasing the observational weight, the reduction of cost function becomes faster (Figure 8b). In other words, the higher the precision of observation error, the faster the cost function converges. It is worth noticing that the minimization process stopped after 8 or 9 iterations with the small weight of observational error (for instance, ratio <1). On the contrary, the minimization process stopped with only ~40% reduction after 35 iterations, while the weight of observation error was assigned by 0.5×10^7 mm^{-2}. This demonstrates that the minimization procedure of the MM5-4DVAR system works well with the higher precision of observation error. When we chose the small weight of observation error, the minimization process stopped with a small amount of cost function reduction. The deviation of the "optimal" initial condition and its impact on the forecast results will be discussed in the following section.

[30] Figure 8c shows that the reduction of the gradient norm is quite different from the reduction of cost function. The gradient norm shows large fluctuations with respect to the iteration number. However, the reduction of gradient norm in all of the experiments exceeds 80% of its initial value in the different weight experiments after 25 iterations. The reduction of gradient norm is not as sensitive to the weight of observational error as the reduction of the cost function is.

[31] During the minimization procedure for the different weight of observation error, the major reductions of the cost function occur in the first five iterations. After 25 iterations, the reductions are minimal, which demonstrates that the minimization procedure of the MM5 adjoint system works well in all of the experiments. In the small weight of observation (for instance, the weight of 0.5×10^7), the reduction of cost function does not exceed 50% of the initial value.

5.2.2. Rainfall Forecast

[32] In this case (Case 2), rainfall is concentrated over the Mogollon Rim mountainous areas in northern Arizona. In order to examine the effects of the observational rainfall error specification in the assimilation processes and subsequent prediction, we conduct a sensitivity study of the rainfall forecasts for the first 6 hours and the second 6 hours to the 4DVAR analyses with different observational error weighting. For the first 6-hour forecast, NO4DVAR does not pick up the two rainfall bands of the storm (Figure 9a versus Figure 9b). In contrast, with the averaged results of these different weighting 4DVAR experiments, the forecasts greatly catch the rainfall bands over most of northeastern Arizona (compared among Figures 9a, 9b, and 9c). The rainfall forecasts in the second 6-hour period indicate that the NO4DVAR experiment produces a strong rainfall center in central Arizona (Figure 9e), which is totally different from the observation with four rainfall bands over the Arizona and New Mexico areas (Figure 9d). The rainfall forecasts from the 4DVAR experiments (Figure 9f) possess better patterns and much reduced rainfall amounts compared to the NO4DVAR experiment over the central Arizona areas, although they are not completely consistent with the observation.

[33] It is clearly shown that the 4DVAR simulates the improvement of the rainfall location with northward and southward rainbands. The 4DVAR also produces less rainfall amounts over western Arizona; however, there is still a northward shift in terms of the position of the rainband. The 4DVAR simulates relatively proper locations of the rainband but misses the rainfall maximum center. This suggests that the assimilation of the rainfall plays an important role in the simulation of the rainband. Observational rainfall can correct the rainfall location in the 4DVAR experiment, although it shifts the location of the maximum rain north-

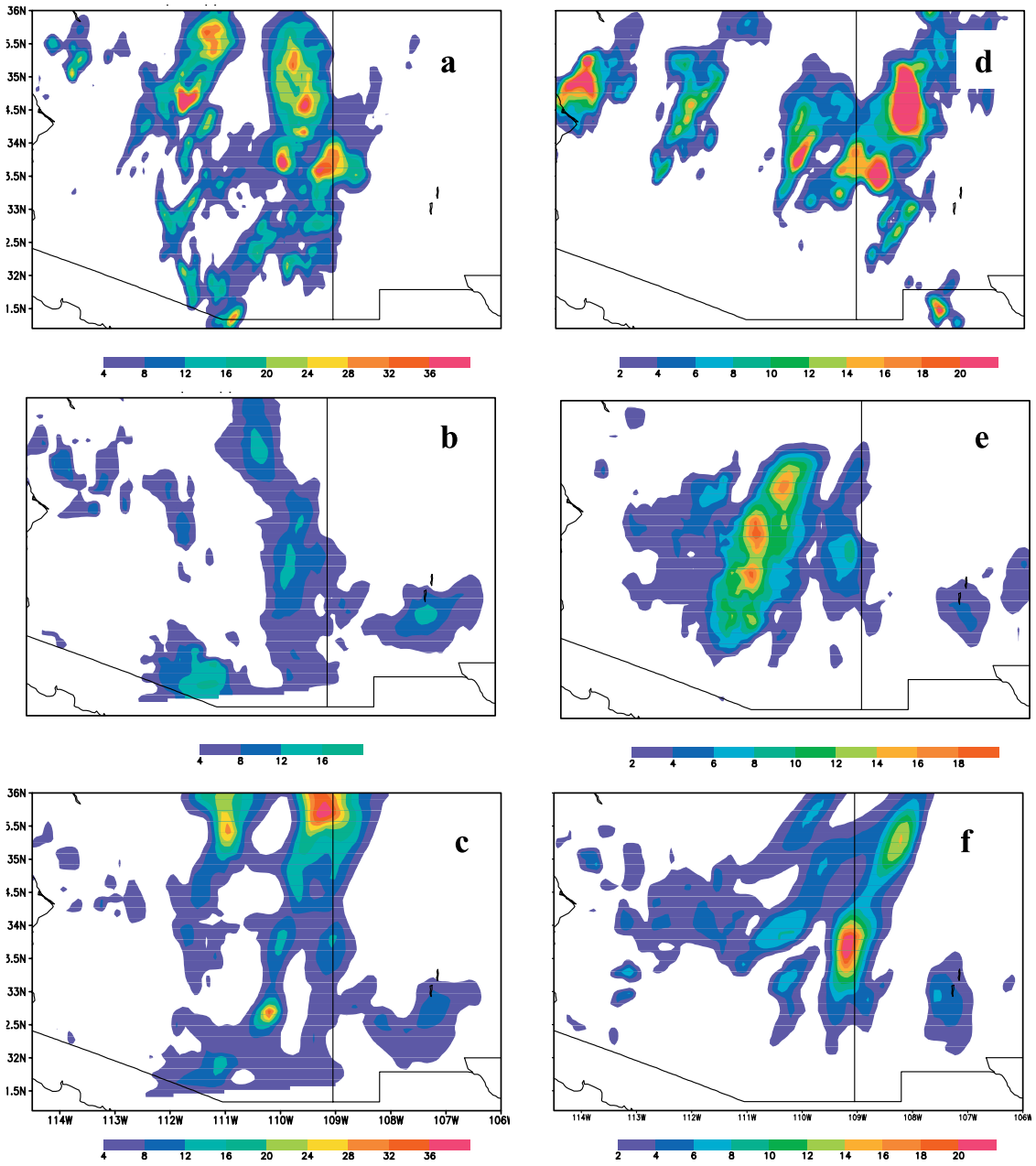

Figure 9. Six-hour accumulated precipitation (mm) at 0600 UTC 11 September 2002 from (a) observation, (b) NO4DVAR, and (c) 4DVAR and at 1200 UTC 11 September 2002 from (d) observation, (e) NO4DVAR, and (f) 4DVAR.

eastward. Considering the passage of mesoscale convective systems over the mountainous areas, a large amount of heavy rainfall could occur in the western slope of mountainous regions. In this respect, the 4DVAR experiment simulates a possible rainband extension toward the western slope regions through the Mogollon Rim mountainous areas.

5.2.3. Statistical Analysis

[34] To examine the effect of the 4DVAR analysis on the rainfall prediction, five statistical variables—mean, root-mean-square error (RMSE), correlation coefficient, bias, and equitable threat score (ETS)—are calculated against the observational rainfall data over the rainstorm central areas (the heavy box in Figure 6a). The mean of forecast precipitation (Figure 10a) either with or without 4DVAR is less than the observation. The correlation coefficient retains 0.35 from the 6-hour to the 12-hour forecast in the 4DVAR experiment (Figure 10b), which is higher than the value in the NO4DVAR. The RMSE (Figure 10c) and bias (Figure 10d) show that the forecast errors in the 4DVAR experiment are smaller than the counterpart in the NO4DVAR experiment before the 15-hour forecast.

[35] The equitable threat score (ETS) is calculated for all of the experiments to verify against the observations. The results for the precipitation thresholds of 4 mm are presented in Figure 10e. Without rainfall assimilation, the ETS

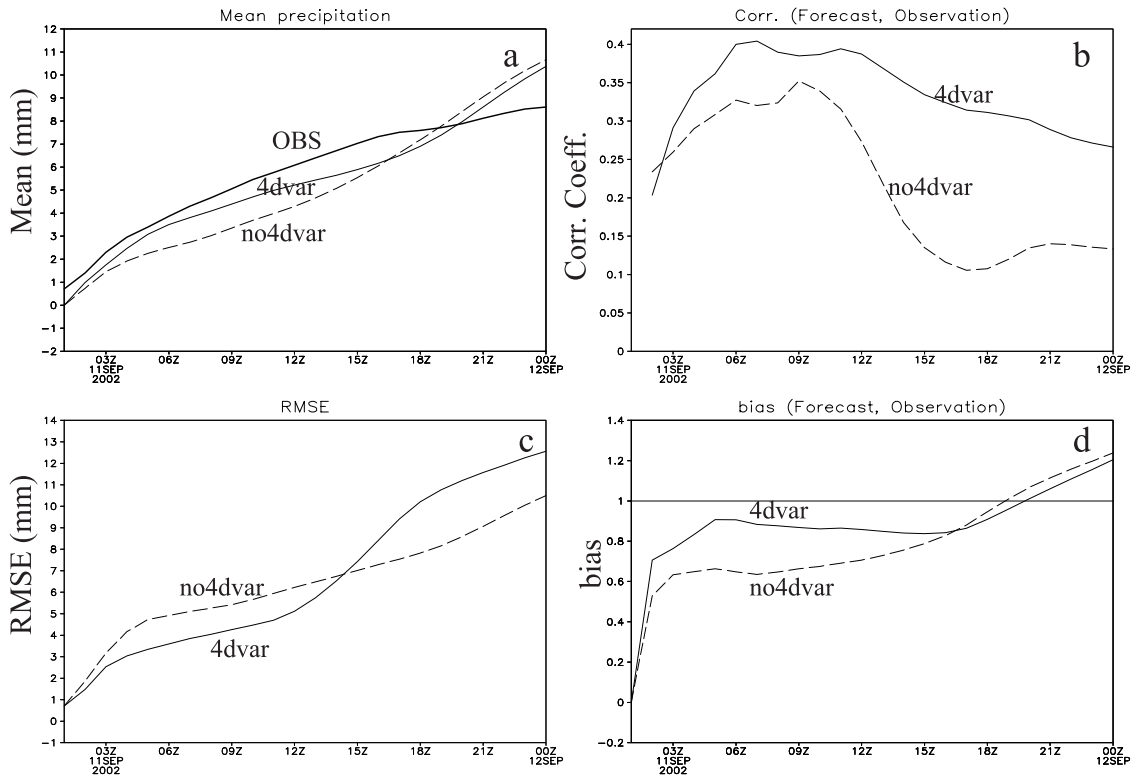

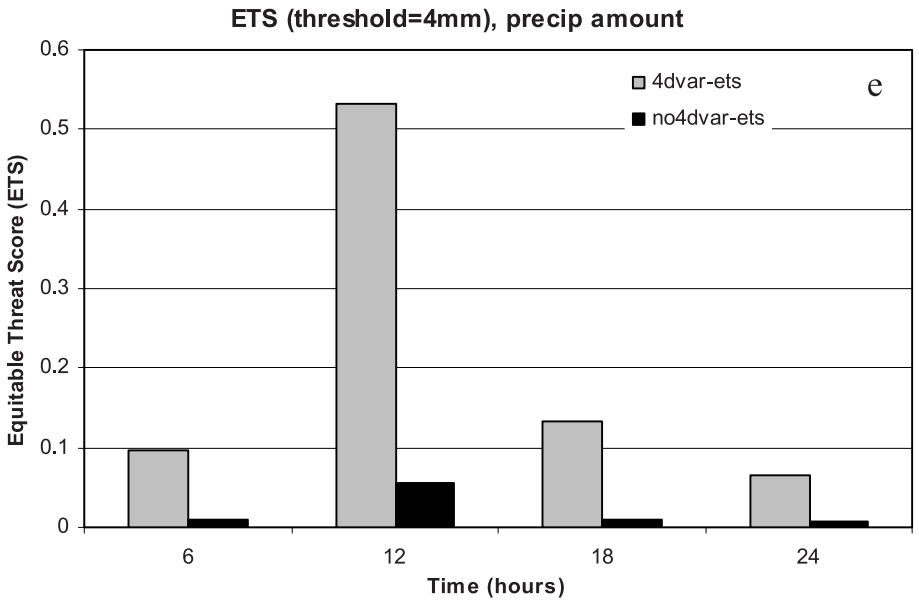

Figure 10. Time series of statistical variables for precipitation (a) mean, (b) correlation coefficient, (c) root-mean-square error (RMSE), (d) bias, and (e) equitable threat score (ETS).

is close to zero from the 6-hour to the 24-hour forecast. The improvement on the rainfall prediction through 4DVAR extends beyond the 12-hour forecast. The highest threat score is obtained in the 12-hour forecast in the 4DVAR experiment.

[36] From these statistical results (Figures 10a–10e), it is suggested that assimilation of rainfall produces better short-range precipitation forecasts. The improvement is mainly limited to the forecast range of about 15 hours in this case study.

6. Analyses

[37] In the 4DVAR assimilation experiments, sophisticated moist physics are used, including the *Grell* [1993] cumulus parameterization scheme and *Dudhia*'s [1993] explicit

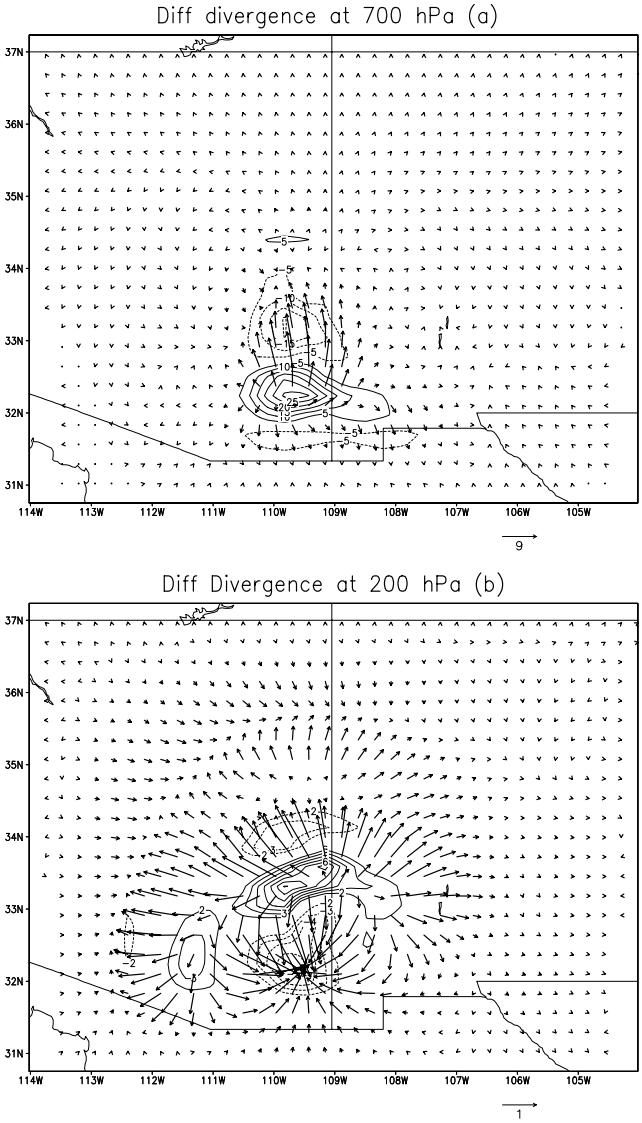

Figure 11. Difference of initial field between the 4DVAR results and original analysis (NO4DVAR): divergence field (countours, units 10^{-5}/s), moisture transport vector ($\mathbf{u} \times \mathbf{q}$; $\mathbf{v} \times \mathbf{q}$) (units g/kg × m/s) at (a) 700 hPa and (b) 200 hPa.

moisture (cloud and rainwater) scheme in the minimization process. Because both schemes are suitable for small-scale convection, the 4DVAR assimilation of rainfall results in improved rainfall forecasts. How does the assimilation process improve the rainfall forecast? The model results from the 4DVAR experiment RAD6H are used to explore the insight processes.

6.1. Initial Conditions

[38] The 4DVAR system seeks the optimal ICs for numerical weather forecasts by adjusting the model ICs to make the prediction match the observed rainfall (hourly) data during the assimilation window. The MM5 model dynamics and physics serve as a strong constraint for the adjusted fields at the initial time (2100 UTC). The differences between the optimal ICs and original ICs are shown in Figure 11. It is indicated that assimilation of the hourly rainfall data results in low level (700 hPa) divergence (Figure 11a) and upper level (200 hPa) convergence (Figure 11b) over eastern Tucson, where storms are observed (Figure 1b). The convergence of moisture flow at the lower level in the 4DVAR analysis is reduced, and the overestimated rainfall in the NO4DVAR experiment could be corrected.

6.2. Moisture Transportation

[39] The perturbation fields of moisture transportation and divergence at 700 mb are presented in Figure 12. Here, the perturbation is defined as the difference between the 4DVAR and NO4DVAR values. Because of the hourly rainfall data assimilation, the perturbation fields show a

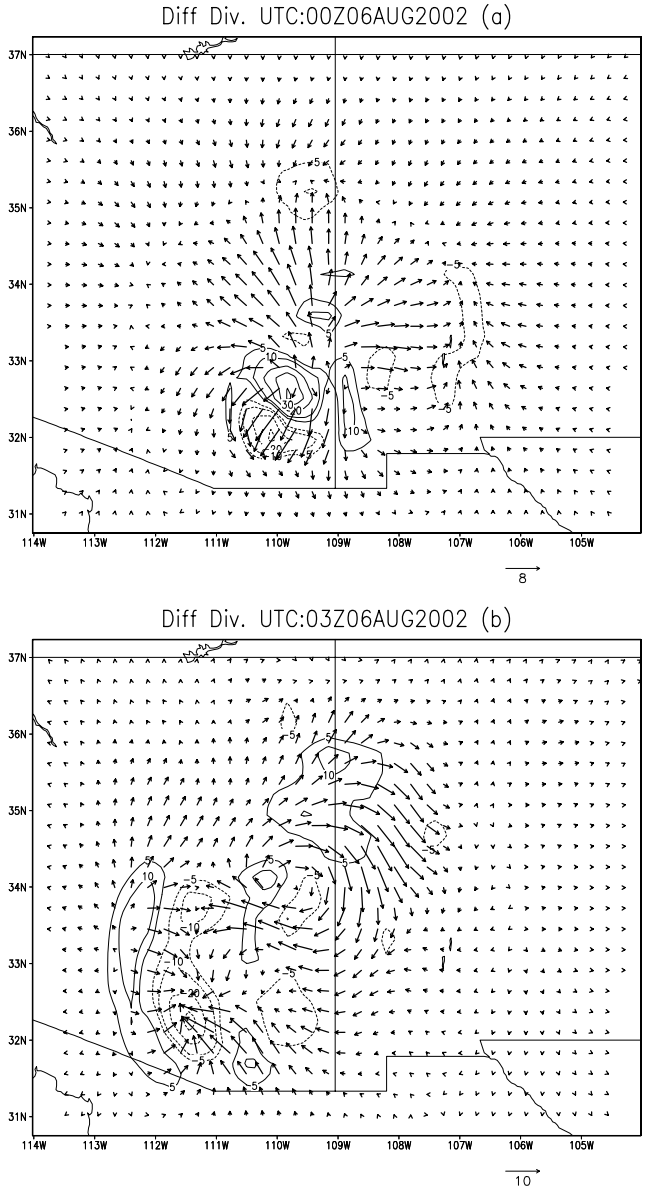

Figure 12. Difference (4DVAR-NO4DVAR) of divergence field (units 10^{-5}/s), moisture transport vector ($\mathbf{u} \times \mathbf{q}$; $\mathbf{v} \times \mathbf{q}$) (units g/kg × m/s) at 700 hPa at (a) 0000 UTC and (b) 0300 UTC 6 August 2002.

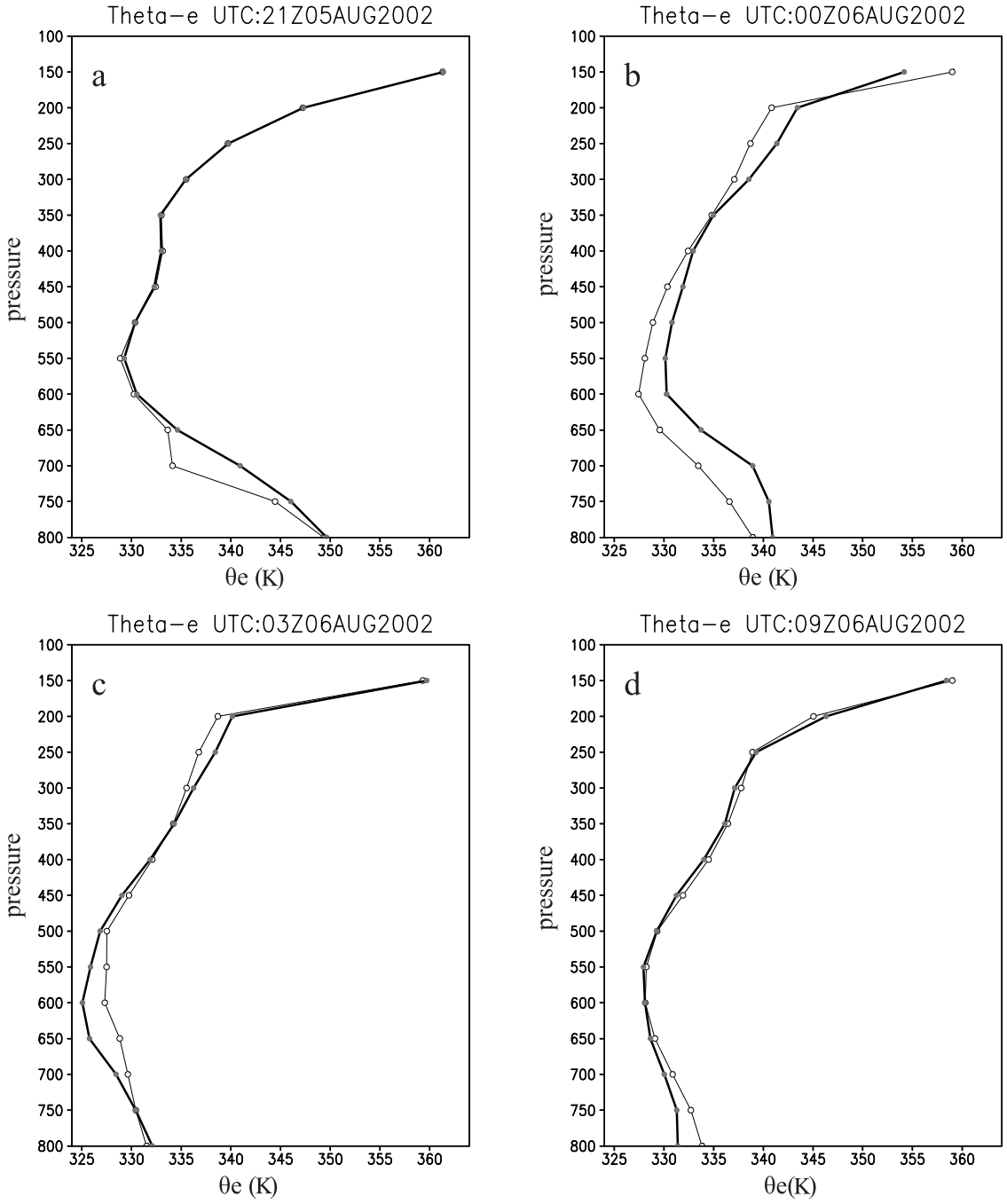

Figure 13. Vertical profile of equivalent potential temperature θ_e (K) over the region (111.5°–109°W, 31.5°–33°N) for (a) 2100 UTC 5 August, (b) 0000 UTC 6 August, (c) 0300 UTC 6 August, and (d) 0900 UTC 6 August 2002 (thin line indicates 4DVAR; thick line represents NO4DVAR).

couplet structure of low level divergence and upper level convergence (Figures 11a and 11b). The couplet structure can reduce atmospheric moisture in the storm active region. During the forecast afterward, the perturbation center of low level divergence moves northward, and a convergence perturbation is built up quickly near Tucson at 0000 UTC 6 August (Figure 12a). The convergence is intensified during the next 3 hours and moves westward (Figure 12b). Accompanying the low level convergence perturbation, there is always a divergence perturbation in the upper level (not shown). This variation of divergence guides the westward moisture transportation to the area where storms are observed.

6.3. Vertical Profile of Equivalent Potential Temperature (θ_e)

[40] The vertical profiles of average θ_e where the storm took place (111.5°–109°W, 31.5°–33°N) are shown in Figure 13. After hourly rainfall data assimilation, the instability layer where the vertical profile of θ_e decreases

with height is from the surface up to 650 mb, much lower than that of the NO4DVAR experiment in the original ICs (Figure 13a). This difference of the θ_e profile persists for several hours (Figure 13b). After six hours, the vertical profiles of θ_e in 4DVAR and NO4DVAR forecasts become almost identical (Figures 13c and 13d). A lower instability layer reduces the convective available potential energy (CAPE) and produces less rainfall in the convective event.

6.4. Vertical Motion

[41] Vertical motion is closely related to rainfall production. To examine the change of the vertical motion after rainfall assimilation, the wind component on the vertical cross section that crossed through the rain center at 32°N from 104°W to 114°W is examined. At the initial time of the 4DVAR experiment, the upward motion has a maximum speed of 30 cm/s at 109.5°W (Figure 14a), which is consistent with the location where storms occurred (Figure 1d). Three hours later, the upward motion is intensified: the maximum speed increases to 160 cm/s and moves westward to around 111°W (Figure 14b). Afterward, the upward motion continues moving westward, but becomes slightly weaker (Figure 14c). This is a strong vertical wind (mean) for an atmosphere column with a 20-km diameter (the horizontal resolution of the simulations). Such strong vertical motion is from not only the dynamic adjustments, but also the release of rainfall latent heat in the atmospheric column through the rainfall assimilation. Meanwhile, a weak downward motion is found on the eastern side of the upward motion, which indicates the asymmetric secondary circulation feature of the convective storms.

[42] The differences of vertical velocity between the 4DVAR and NO4DVAR wind fields are represented in Figures 14d–14f. Because of the rainfall assimilation, the initial upward motion is reduced slightly over the region where the storm began (Figure 14d). Three hours later, the reduction increases to 100 cm/s over the same area, while an increase of upward motion appears on the west side of the reduction column (Figure 14e). The similar pattern persists for several hours (Figure 14f). This result shows that the upward motion is modified substantially after the rainfall assimilation. The evolution of the upward motion matches well with the observed storm activity in the area.

7. Summary and Discussion

7.1. Summary

[43] Two convective storm events that occurred over the mountainous southwestern United States on 5–6 August and 11–12 September 2002 are used for a series of rainfall assimilation experiments with the full physics mesoscale data assimilation system MM5-4DVAR. In order to understand the effects of rainfall assimilation on the subsequent forecasts over the mountainous region, both 3-hour and 6-hour assimilation windows are tested, and different weightings of rainfall observation error are examined. The minimization algorithm used in these studies is the limited-memory quasi-Newton method developed by *Liu and Nocedal* [1989]. The NCEP operational Eta analysis provides the first guess in the minimization procedure. After obtaining the optimal initial conditions, numerical forecasts using MM5 version 3.5 are carried out for 24 hours from the initial time. The results are summarized as follows:

[44] The minimization procedure of the MM5-4DVAR system works well in the rainstorm event over a mountainous area of the southwestern United States. It indicates that 20 iterations are sufficient for convergence of the 4DVAR process in rainfall assimilation. However, the specified errors of the rainfall observation and the length of the assimilation window have strong influences on the convergence of the minimization procedure.

[45] The effective forecast duration is sensitive to the length of the window. A 3-hour assimilation window works well for 6-hour forecasts at 20-km model resolution. When 12-hour or longer forecasts are made, a 6-hour assimilation window is needed. These results could be found in these two cases studies.

[46] Rainfall assimilation in the MM5-4DVAR shows the capability of modifying the initial conditions, and it generates more realistic moisture divergence, temperature fields, instability, and vertical motion. Mesoscale weather forecasts from the optimal initial conditions reproduce the storm pattern and quantity closer to the observations than the NO4DVAR results.

[47] The 4DVAR rainfall assimilation is sensitive to the specified error of the observation data. The quality of observed rainfall data in assimilation has significant impacts on the improvement of the initial conditions and therefore the forecasts.

7.2. Discussion

[48] In this study, the rainfall assimilation using the MM5-4DVAR system is shown to improve the rainstorm forecasts of the selected two cases over the mountainous areas in the southwestern United States. However, because of the complexity of the parameterization of rainfall processes and the lack of knowledge in the estimation of observational errors, the limitations of rainfall assimilation should be given more attention.

[49] First of all, parameterization of rainfall processes plays a significant role in simulating various large-scale and mesoscale phenomena. They should be correctly incorporated into the adjoint model, which involves the ''on-off'' switches issue [*Xu*, 1996; *Zou*, 1997]. The concern in 4DVAR with the moist physics possessing ''on-off'' switches in the adjoint model is really related to whether the adjoint technique can provide sufficient information for minimization-finding descent directions. The switch on-and-off timing and location of initial precipitation are important to the final results. The difference between forecast field and observed field shown in Figure 9 demonstrates that the rainfall forecast is not completely consistent with the observation, even when the rainfall is assimilated. The on-and-off problem is probably the reason for the inconsistency. To solve this problem, it is better to add other moist data to rainfall observations during the assimilation procedure to reduce the arbitrariness of 4DVAR in adjusting the initial moisture field. *Zou* [1997] pointed out that combining the rainfall observations with wind, temperature, surface moisture, and PW results in better rainfall prediction than the one assimilating only the rainfall observations.

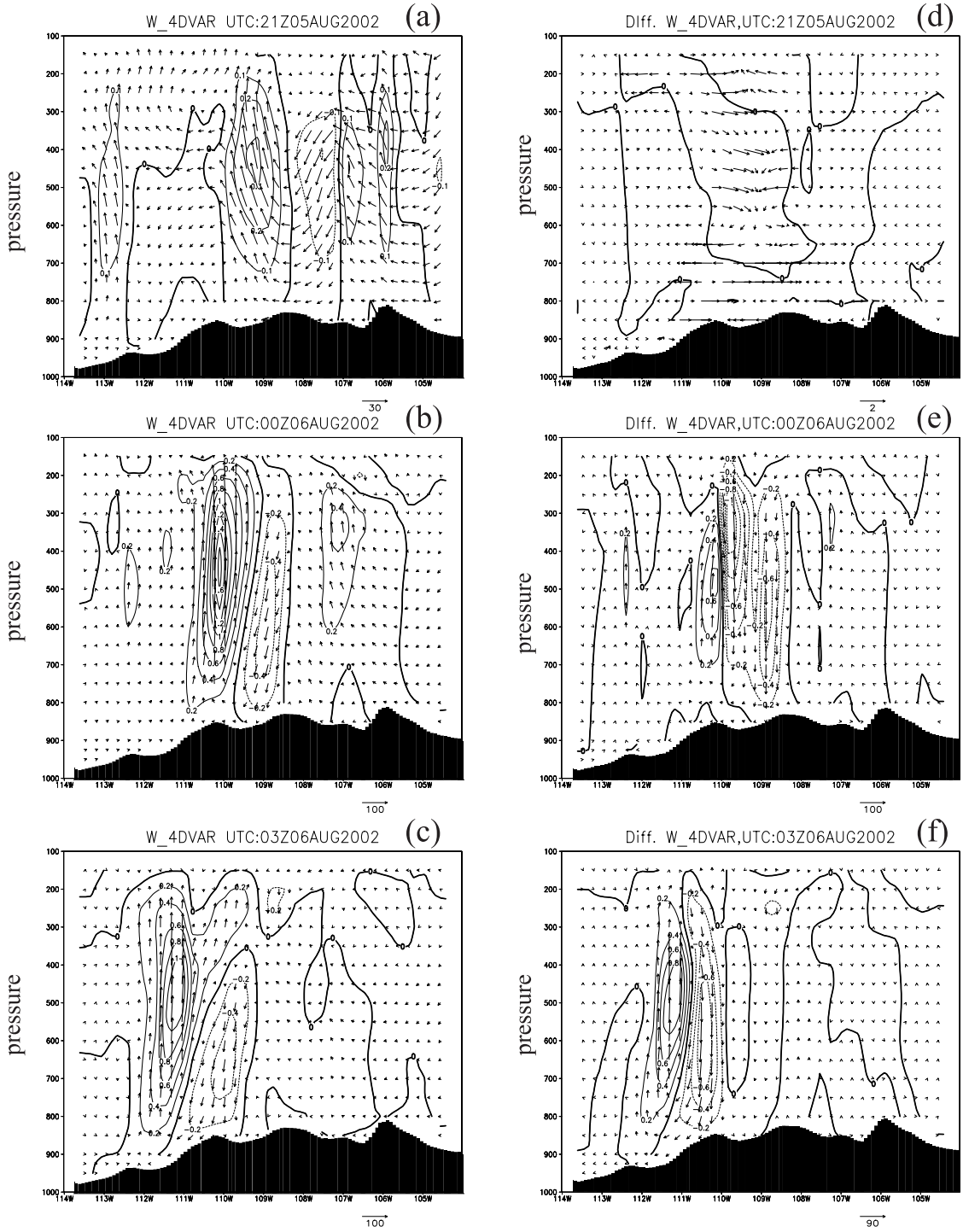

Figure 14. Wind component on the vertical cross section at section 32°N in the 4DVAR experiment for (a) 2100 UTC 5 August, (b) 0000 UTC 6 August, and (c) 0300 UTC 6 August and the difference (4DVAR-NO4DVAR) of the wind component for (d) 2100 UTC 5 August, (e) 0000 UTC 6 August, and (f) 0300 UTC 6 August 2002.

[50] Second, meteorological observations are not perfect; that is, observational errors cannot be neglected. Two types of observational errors are common: random errors and systematic errors, possibly caused by human or instrument errors. Even if the observational instruments were in perfect condition so that there were no systematic errors produced by the instrumentation, representation would still contribute systematic observational errors. The rainfall observation from the WSR-88D radar involves errors from the Doppler radar instrument to the algorithms of processing. In practice, the assignment of the observation error is a very complicated issue. In this paper, we tried a range of rainfall

observation errors in our assimilation experiments and obtained an idea of how large the error should be. Statistical estimation should be done and discussed in future work.

[51] Finally, this conclusion is just from these two cases studies. There is still a great deal of work to be done to improve rainfall data assimilation, although these results in these two cases could be demonstrated to be consistent.

[52] **Acknowledgments.** The authors want to express special thanks to colleagues at the University of Arizona because most of the calculations were completed there. This study is partially sponsored by NASA grant NAG5-11044, NOAA grant NA16GP1605, and NSF/SAHRA ("Sustainability of Semi-Arid Hydrology and Riparian Areas") grant ERA-9876800. The research of Qingnong Xiao is supported by the U.S. Weather Research Program at NCAR.

References

Adams, D. K., and A. C. Comrie (1997), The North American monsoon, *Bull. Am. Meteorol. Soc.*, *78*, 2197–2213.

Alexander, G. D., J. A. Weinman, V. M. Karyampudi, W. S. Olson, and A. C. L. Lee (1999), The effect of assimilating rain rates derived from satellites and lightning on forecasts of the 1993 superstorm, *Mon. Weather Rev.*, *127*, 1433–1457.

Anderson, B., and J. O. Roads (2002), Regional simulation of summertime precipitation over the Southwestern United States, *J. Clim.*, *15*, 3321–3342.

Benjamin, S. O., and N. L. Seaman (1985), A simple scheme for objective analysis in curved flow, *Mon. Weather Rev.*, *113*, 1184–1198.

Colle, B., and C. Mass (1996), An observational and modeling study of the interaction of low-level southwesterly flow with the Olympic Mountains during COAST IOP 4, *Mon. Weather Rev.*, *124*, 2152–2175.

Davidson, N. E., and K. Puri (1992), Tropical prediction using dynamical nudging, satellite-defined convective heat sources, and a cyclone bogus, *Mon. Weather Rev.*, *120*, 2501–2522.

De Pondeca, M., and X. Zou (2001), A case study of the variational assimilation of GPS zenith delay observations into a mesoscale model, *J. Appl. Meteorol.*, *40*, 1559–1576.

Desroziers, G., and S. Ivanov (2001), Diagnosis and adaptive tuning of observation-error parameters in a variational assimilation, *Q. J. R. Meteorol. Soc.*, *127*, 1433–1452.

Douglas, M. W., R. A. Maddox, K. W. Howard, and S. Reyes (1993), The Mexican monsoon, *J. Clim.*, *6*, 1665–1677.

Dudhia, J. (1989), Numerical study of convection observed during the winter monsoon experiment using a mesoscale two-dimensional model, *J. Atmos. Sci.*, *46*, 3077–3107.

Dudhia, J. (1993), A nonhydrostatic version of the Penn State/NCAR mesoscale model: Validation tests and simulation of an Atlantic cyclone and cold front, *Mon. Weather Rev.*, *121*, 1493–1513.

Farfan, L. M., D. R. Bright, and J. A. Zehnder (1998), Numerical simulation of mesoscale weather system in Arizona, paper presented at 12th Conference on Numerical Weather Prediction, Am. Meteorol. Soc., Phoenix, Ariz.

Fulton, R. A., J. P. Breidenbach, D.-J. Seo, D. A. Miller, and T. O'Bannon (1998), The WSR-88D rainfall algorithm, *Weather Forecasting*, *13*, 377–395.

Grell, G. (1993), Prognostic evaluation of assumptions used by cumulus parameterizations, *Mon. Weather Rev.*, *121*, 764–787.

Grell, G. A., J. Dudhia, and D. R. Stauffer (1994) A description of the fifth-generation Penn State/NCAR mesoscale model (MM5), *NCAR Tech. Note NCAR/TN-398+STR*, 117 pp., Natl. Cent. for Atmos. Res., Boulder, Colo.

Le Dimet, F. X., and O. Talagrand (1986), Variational algorithms for analysis and assimilation of meteorological observations: Theoretical aspects, *Tellus, Ser. A*, *38*, 97–110.

Lewis, J. M., and J. C. Derber (1985), The use of adjoint equations to solve a variational adjustment problem with advective constraints, *Tellus, Ser. A*, *37*, 309–322.

Li, Z., I. M. Navon, and Y. Zhu (2000), Performance of 4D-Var with different strategies for the use of adjoint physics with the FSU global spectral model, *Mon. Weather Rev.*, *128*, 668–688.

Liu, D. C., and J. Nocedal (1989), On the limited memory BFGS method for large-scale optimization, *Math. Program.*, *45*, 503–528.

Lorenz, E. N. (1963), The mechanics of vacillation, *J. Atmos. Sci.*, *20*, 448–465.

Maddox, R. A., J. Z. J. Gourley, and K. W. Howard (2002), Weather radar coverage over the contiguous United States, *Weather Forecasting*, *17*, 927–934.

Negri, A. J., and R. F. Adler (1993), An intercomparison of three satellite infrared rainfall techniques over Japan and surrounding waters, *J. Appl. Meteorol.*, *32*, 357–373.

Negri, A. J., R. F. Adler, E. J. Nelkin, and G. J. Huffman (1994), Regional rainfall climatologies derived from special sensor microwave imager (SSM/I) data, *Bull. Am. Meteorol. Soc.*, *75*, 1165–1182.

Okabe, I. T. (1994), The North American monsoon, Ph.D. dissertation, Univ. of B.C., 146 pp., Vancouver, B. C., Canada.

Petty, G. W., and D. K. Miller (1995), Satellite microwave observations of precipitation correlated with intensification rate in extratropical oceanic cyclones, *Mon. Weather Rev.*, *123*, 1904–1911.

Smith, J. A., and W. Krajewski (1991), Estimation of the mean field bias of radar rainfall estimates, *J. Appl. Meteorol.*, *30*, 397–412.

Smith, R. B. (1979), The influence of mountains on the atmosphere, *Adv. Geophys.*, *21*, 87–230.

Stensrud, D. J., and J.-W. Bao (1992), Behaviors of variational and nudging assimilation techniques with a chaotic low-order model, *Mon. Weather Rev.*, *120*, 3016–3028.

Stensrud, D. J., R. L. Gall, S. L. Mullen, and K. W. Howard (1995), Model climatology of the Mexican monsoon, *J. Clim.*, *8*, 1775–1794.

Talagrand, O., and P. Courtier (1987), Variational assimilation of meteorological observations with the adjoint vorticity equation. part I: Theory, *Q. J. R. Meteorol. Soc.*, *113*, 1313–1330.

Toth, Z., and E. Kalnay (1993), Ensemble forecasting at NMC: The generation of perturbations, *Bull. Am. Meteorol. Soc.*, *74*, 2317–2330.

Tsuyuki, T. (1997), Variational data assimilation in the tropics using precipitation data. part III: Assimilation of SSM/I precipitation rates, *Mon. Weather Rev.*, *125*, 1447–1463.

Uccellini, L. W. (1991), Processes contributing to the rapid development of extratropical cyclones, in *Extratropical Cyclones: Erik Palmen Memorial Volume*, edited by C. W. Newton and E. Holopainen, pp. 166–191, Am. Meteorol. Soc., Boston, Mass.

Vukicevic, T., and J.-W. Bao (1998), The effect of linearization errors on 4DVAR data assimilation, *Mon. Weather Rev.*, *126*, 1695–1706.

Xiao, Q., X. Zou, and Y.-H. Kuo (2000), Incorporating the SSM/I derived precipitable water and rainfall rate into a numerical model: A case study for ERICA IOP-4 cyclone, *Mon. Weather Rev.*, *128*, 87–108.

Xu, J., and E. E. Small (2002), Simulating summertime rainfall variability in the North American monsoon region: The influence of convection and radiation parameterizations, *J. Geophys. Res.*, *107*(D23), 4727, doi:10.1029/2001JD002047.

Xu, J., X. Gao, J. Shuttleworth, S. Sorooshian, and E. Small (2004a), Model climatology of the North American monsoon onset period during 1980–2001, *J. Clim.*, *17*, 3892–3906.

Xu, J., X. Gao, Q. Xiao, and S. Sorooshian (2004b), Investigate the impacts of assimilating satellite rainfall estimates on rainstorm forecast over southwest United States, *Geophys. Res. Lett.*, *31*, L16104, doi:10.1029/2004GL020120.

Xu, Q. (1996), Generalized adjoint for physical processes with parameterized discontinuities, part I: Basic issues and heuristic examples, *J. Atmos. Sci.*, *53*, 1123–1142.

Zeng, X., and E. Lu (2004), Globally unified monsoon onset and retreat indexes, *J. Clim.*, *17*, 2241–2248.

Zou, X. (1997), Tangent linear and adjoint of "on-off" processes and their feasibility for use in 4-dimensional variational data assimilation, *Tellus, Ser. A*, *49*, 3–31.

Zou, X., and Y.-H. Kuo (1996), Rainfall assimilation through an optimal control of initial and boundary conditions in a limited-area mesoscale model, *Mon. Weather Rev.*, *124*, 2859–2882.

Zou, X., W. Huang, and Q. Xiao (1998), A user's guide to the MM5 adjoint modeling system, *NCAR Tech. Note TN-437+IA*, 1070 pp., Natl. Cent. for Atmos. Res., Boulder, Colo.

Zupanski, D., and F. Mesinger (1995), Four-dimensional variational assimilation of precipitation data, *Mon. Weather Rev.*, *123*, 1112–1127.

X. Gao and S. Sorooshian, Department of Civil and Environmental Engineering, University of California, Irvine, CA 92697-2175, USA.

Q. Xiao, National Center for Atmospheric Research, Boulder, CO 80305, USA.

J. Xu, Joint Center for Satellite Data Assimilation, 5200 Auth Road, WWB, Camp Springs, MD 20746, USA. (jianjun.xu@noaa.gov)